Novel focused OCT-LIF endoscope

R. Andrew Wall,[1] Garret T. Bonnema,[1] and Jennifer K. Barton[1,2,*]

[1]*College of Optical Sciences, The University of Arizona, 1230 East Speedway Boulevard, Tucson, Arizona 85721, USA*
[2]*Department of Biomedical Engineering, The University of Arizona, 1230 East Speedway Boulevard, Tucson, Arizona 85721, USA*
**barton@u.arizona.edu*

Abstract: Combined optical coherence tomography (OCT) and laser-induced fluorescence (LIF) endoscopy has shown higher sensitivity and specificity for distinguishing normal tissue from adenoma when compared to either modality alone. Endoscope optical design is complicated by the large wavelength difference between the two systems. A new high-resolution endoscope 2 mm in diameter is presented that can create focused beams from the ultraviolet to near-infrared. A reflective design ball lens operates achromatically over a large wavelength range, and employs TIR at two faces and reflection at a third internal mirrored face. The 1:1 imaging system obtains theoretically diffraction-limited spots for both the OCT (1300 nm) and LIF (325 nm) channels.

OCIS codes: (120.3890) Medical optics instrumentation; (170.2150) Endoscopic imaging; (170.2680) Gastrointestinal; (170.4500) Optical coherence tomography; (170.6280) Spectroscopy, fluorescence, and luminescence.

References and links

1. *Cancer Facts & Figs, 2010* (American Cancer Society, Atlanta, Georgia, 2009). http://www.cancer.org/downloads/STT/Cancer_Facts_and_Figures_2010.pdf.
2. A. Das, M. V. Sivak, Jr., A. Chak, R. C. Wong, V. Westphal, A. M. Rollins, J. Willis, G. Isenberg, and J. A. Izatt, "High-resolution endoscopic imaging of the GI tract: a comparative study of optical coherence tomography versus high-frequency catheter probe EUS," Gastrointest. Endosc. **54**(2), 219–224 (2001).
3. B. E. Bouma, and G. J. Tearney, eds., *Handbook of Optical Coherence Tomography* (Marcel Dekker, New York, 2002).
4. D. Huang, E. A. Swanson, C. P. Lin, J. S. Schuman, W. G. Stinson, W. Chang, M. R. Hee, T. Flotte, K. Gregory, and C. A. Puliafito, "Optical coherence tomography," Science **254**(5035), 1178–1181 (1991).
5. M. V. Sivak, Jr., K. Kobayashi, J. A. Izatt, A. M. Rollins, R. Ung-Runyawee, A. Chak, R. C. Wong, G. A. Isenberg, and J. Willis, "High-resolution endoscopic imaging of the GI tract using optical coherence tomography," Gastrointest. Endosc. **51**(4), 474–479 (2000).
6. E. Zagaynova, N. Gladkova, N. Shakhova, G. Gelikonov, and V. Gelikonov, "Endoscopic OCT with forward-looking probe: clinical studies in urology and gastroenterology," J Biophotonics **1**(2), 114–128 (2008).
7. D. C. Adler, C. Zhou, T. H. Tsai, J. Schmitt, Q. Huang, H. Mashimo, and J. G. Fujimoto, "Three-dimensional endomicroscopy of the human colon using optical coherence tomography," Opt. Express **17**(2), 784–796 (2009).
8. A. R. Tumlinson, B. Povazay, L. P. Hariri, J. McNally, A. Unterhuber, B. Hermann, H. Sattmann, W. Drexler, and J. K. Barton, "In vivo ultrahigh-resolution optical coherence tomography of mouse colon with an achromatized endoscope," J. Biomed. Opt. **11**(6), 064003 (2006).
9. L. P. Hariri, A. R. Tumlinson, N. H. Wade, D. G. Besselsen, U. Utzinger, E. W. Gerner, and J. K. Barton, "Ex vivo optical coherence tomography and laser-induced fluorescence spectroscopy imaging of murine gastrointestinal tract," Comp. Med. **57**(2), 175–185 (2007).
10. L. P. Hariri, Z. Qiu, A. R. Tumlinson, D. G. Besselsen, E. W. Gerner, N. A. Ignatenko, B. Povazay, B. Hermann, H. Sattmann, J. McNally, A. Unterhuber, W. Drexler, and J. K. Barton, "Serial endoscopy in azoxymethane treated mice using ultra-high resolution optical coherence tomography," Cancer Biol. Ther. **6**(11), 1753–1762 (2007).
11. R. Richards-Kortum, R. P. Rava, R. E. Petras, M. Fitzmaurice, M. Sivak, and M. S. Feld, "Spectroscopic diagnosis of colonic dysplasia," Photochem. Photobiol. **53**(6), 777–786 (1991).
12. A. Lucas, M. J. Radosavljevic, E. Lu, and E. J. Gaffney, "Characterization of human coronary artery atherosclerotic plaque fluorescence emission," Can. J. Cardiol. **6**(6), 219–228 (1990).

#134844 - $15.00 USD Received 14 Sep 2010; revised 4 Nov 2010; accepted 28 Jan 2011; published 31 Jan 2011

13. J. J. Baraga, R. P. Rava, P. Taroni, C. Kittrell, M. Fitzmaurice, and M. S. Feld, "Laser induced fluorescence spectroscopy of normal and atherosclerotic human aorta using 306-310 nm excitation," Lasers Surg. Med. **10**(3), 245–261 (1990).
14. N. Ramanujam, "Fluorescence spectroscopy of neoplastic and non-neoplastic tissues," Neoplasia **2**(1/2), 89–117 (2000).
15. A. L. Alexander, C. M. Connor Davenport, and A. F. Gmitro, "Comparison of illumination wavelengths for detection of atherosclerosis by optical fluorescence spectroscopy," Opt. Eng. **33**(1), 167 (1994).
16. R. L. Prosst, and J. Gahlen, "Fluorescence diagnosis of colorectal neoplasms: a review of clinical applications," Int. J. Colorectal Dis. **17**(1), 1–10 (2002).
17. M. Hassan, and B. A. Klaunberg, "Biomedical applications of fluorescence imaging *in vivo*," Comp. Med. **54**(6), 635–644 (2004).
18. S. Fu, C. T. Chia, C. L. Tang, C. H. Diong, and C. Seow, "Changes in *in-vivo* autofluorescence spectra at different periods in rat colorectal tumor progression," Proc. SPIE **4432**, 118–123 (2001).
19. E. M. Kanter, R. M. Walker, S. L. Marion, M. Brewer, P. B. Hoyer, and J. K. Barton, "Dual modality imaging of a novel rat model of ovarian carcinogenesis," J. Biomed. Opt. **11**(4), 041123 (2006).
20. L. P. Hariri, A. R. Tumlinson, D. G. Besselsen, U. Utzinger, E. W. Gerner, and J. K. Barton, "Endoscopic optical coherence tomography and laser-induced fluorescence spectroscopy in a murine colon cancer model," Lasers Surg. Med. **38**(4), 305–313 (2006).
21. Y. Luo, P. J. Gelsinger-Austin, J. M. Watson, G. Barbastathis, J. K. Barton, and R. K. Kostuk, "Laser-induced fluorescence imaging of subsurface tissue structures with a volume holographic spatial-spectral imaging system," Opt. Lett. **33**(18), 2098–2100 (2008).
22. L. P. Hariri, E. R. Liebmann, S. L. Marion, P. B. Hoyer, J. R. Davis, M. A. Brewer, and J. K. Barton, "Simultaneous optical coherence tomography and laser induced fluorescence imaging in rat model of ovarian carcinogenesis," Cancer Biol. Ther. **10**(5), 438–447 (2010).
23. R. V. Kuranov, V. V. Sapozhnikova, H. M. Shakhova, V. M. Gelikonov, E. V. Zagainova, and S. A. Petrova, "Combined application of optical methods to increase the information content of optical coherent tomography in diagnostics of neoplastic processes," Quantum Electron. **32**(11), 993–998 (2002).
24. J. K. Barton, A. Tumlinson, and U. Utzinger, "Combined endoscopic optical coherence tomography and laser induced fluorescence," in *Optical Coherence Tomography: Technology and Applications*, W. Drexler and J. Fujimoto, eds. (Springer, 2008).
25. S. Y. Ryu, H. Y. Choi, J. Na, E. S. Choi, and B. H. Lee, "Combined system of optical coherence tomography and fluorescence spectroscopy based on double-cladding fiber," Opt. Lett. **33**(20), 2347–2349 (2008).
26. J. B. McNally, N. D. Kirkpatrick, L. P. Hariri, A. R. Tumlinson, D. G. Besselsen, E. W. Gerner, U. Utzinger, and J. K. Barton, "Task-based imaging of colon cancer in the Apc(Min/+) mouse model," Appl. Opt. **45**(13), 3049–3062 (2006).
27. A. R. Tumlinson, L. P. Hariri, U. Utzinger, and J. K. Barton, "Miniature endoscope for simultaneous optical coherence tomography and laser-induced fluorescence measurement," Appl. Opt. **43**(1), 113–121 (2004).
28. J. A. Izatt, M. D. Kulkarni, S. Yazdanfar, J. K. Barton, and A. J. Welch, "*In vivo* bidirectional color Doppler flow imaging of picoliter blood volumes using optical coherence tomography," Opt. Lett. **22**(18), 1439–1441 (1997).
29. T. J. Pfefer, L. S. Matchette, and R. Drezek, "Influence of illumination-collection geometry on fluorescence spectroscopy in multilayer tissue," Med. Biol. Eng. Comput. **42**(5), 669–673 (2004).
30. T. J. Pfefer, L. S. Matchette, A. M. Ross, and M. N. Ediger, "Selective detection of fluorophore layers in turbid media: the role of fiber-optic probe design," Opt. Lett. **28**(2), 120–122 (2003).
31. T. J. Pfefer, K. T. Schomacker, M. N. Ediger, and N. S. Nishioka, "Multiple-fiber probe design for fluorescence spectroscopy in tissue," Appl. Opt. **41**(22), 4712–4721 (2002).
32. R. R. Shannon, "Aberrations," in *The Art and Science of Optical Design* (Cambridge University Press, 2006).
33. J. Sasian, "Optical Design with Mirrors," presented at Optical Design and Testing Short Course Program, Kyoto, Japan, 15–16 November 1997.
34. Eksma Optics, "Metallic Coatings," http://www.eksmaoptics.com/en/p/metallic-coatings-35
35. E. Hecht, "Propagation of light," in *Optics, 4th ed.* (Addison Wesley, 2001).
36. S. W. Smith, "Special imaging techniques," in *The Scientist and Engineer's Guide to Digital Signal Processing* (California Technical Publishing, 1997), pp. 423–430.
37. A. Douplik, D. Chen, M. K. Akens, S. Zanati, M. Cirocco, N. Bassett, N. E. Marcon, J. Fengler, and B. C. Wilson, "Assessment of photobleaching during endoscopic autofluorescence imaging of the lower GI tract," Lasers Surg. Med. **42**(3), 224–231 (2010).

1. Introduction

Colonoscopy is the most commonly used technique for early detection of colorectal cancer, which is the third most common type of cancer in the United States. In 2010, colorectal cancer will be responsible for an estimated 9% of newly diagnosed cancers and cancer related deaths. While the 5-year survival is 90% when these cancers are detected at an early, localized stage, only 40% of patients are diagnosed early [1]. A need exists for rapid, non-destructive visualization of tissues *in vivo*, for clinical diagnostics as well as for scientific study, in order

#134844 - $15.00 USD Received 14 Sep 2010; revised 4 Nov 2010; accepted 28 Jan 2011; published 31 Jan 2011

to make significant advances in the basic science of chemoprevention and chemotherapy. Colonoscopy, while capable of surface visualization, is limited in its ability to detect subsurface pre-cancerous changes. Endoscopic ultrasound is capable of depth-resolved imaging, though its resolution is limited to approximately 110 μm in standard devices [2]. Optical coherence tomography (OCT) is a non-invasive interferometric imaging technique capable of imaging up to 2 mm deep tissue, using backscattered near-infrared light from index of refraction mismatches, to create cross-sectional images [3,4]. Recently, OCT has been used to image the human colon and rectum with micron-scale resolution [5–7]. Mouse models can be utilized to elucidate the genetic and molecular basis of human gastrointestinal disease and to test therapeutic and chemopreventive compounds. We have previously used mice and shown them to be an excellent model for evaluating the use of OCT as a method of detecting colorectal adenomas and monitoring their progression [8–10].

Laser-induced fluorescence (LIF) spectroscopy has demonstrated promising capabilities in the human lung and gastrointestinal tract, showing high sensitivity to neoplastic tissue. Multiple researchers have shown the ability of LIF techniques to identify cancer and neoplastic tissue in human tissue using only endogenous fluorophores [11–17]. We have extended this work past humans as well to show the benefit of using LIF spectroscopy to study the murine model [18–22].

Ultraviolet (UV)-blue light is highly efficient at exciting tissue autofluorescence. At 325 nm, endogenous fluorophores such as the metabolic cofactors hydrogentated nicotinamide adenine dinucleotide and flavin adenine dinucleotide, as well as collagen, can be excited. Exogenous fluorophores, including as those that can target neoplastic cells, are frequently excited with green-red light. Near-infrared (NIR) light centered around 1300 nm offers deep tissue penetration for OCT viewing of more advanced disease. The ability to achromatically focus across this large wavelength range would grant the ability to study the biochemical distribution of the tissue as well as its morphological structure with high resolution.

Combining OCT and LIF in one endoscopic system, with LIF providing information about the biochemical composition and OCT information about tissue boundaries, structure, and thickness, can provide a heightened sensitivity and specificity to tumor detection when compared to either modality alone [23,24]. Previously, we built endoscopes with ultrahigh resolution (2-5 μm) OCT, and high resolution OCT combined with unfocused LIF, and demonstrated imaging of mouse colon [9,25,26]. Unfocused LIF has the disadvantage of illuminating and collecting fluorescence emission from a large tissue volume. Therefore, it can be difficult to compare OCT images and LIF data due to the much larger tissue volumes being interrogated with LIF compared to OCT (approximately 5 μm OCT beam waist vs. 1 mm diameter LIF spot size on the tissue surface). Three-dimensional data sets of the colon can help resolve ambiguities with LIF sensing features outside the field of view of OCT, but smaller LIF spot sizes may also allow detection of early, focal regions of neoplastic change.

Our earliest side-firing endoscopes utilized an optical design consisting of a single-mode fiber glued directly to a gradient-index (GRIN) lens, which was in turn cemented to a prism that redirected the light sideways out of the endoscope window [27]. Chromatic aberration in GRIN lenses, however, precluded their use for simultaneously focusing the LIF UV excitation light as well as the OCT NIR light (the difference in foci for 325 and 1300 nm light for our design is about 0.5 mm). GRIN lenses also exhibit strong autofluorescence when excited in the UV, so the LIF channel in our previous endoscopes bypassed the GRIN lens, and the system was carefully designed to avoid any stray UV light impinging on the GRIN lens. Some achromatic endoscope designs exist, such as the one published by ourselves in 2006 [8], but work over wavelength ranges much smaller (e.g. 400 nm) than the present design and were not meant for multi-modality use.

We have designed and built an endoscope using a reflective ball lens that is capable of focusing light over a range from 325 nm to at least 1300 nm. Reflective optics as opposed to refractive optics are used to remove chromatism from systems. Such designs have yet to be

#134844 - $15.00 USD Received 14 Sep 2010; revised 4 Nov 2010; accepted 28 Jan 2011; published 31 Jan 2011

extensively utilized in biomedical applications. OCT utilizes a focused NIR beam for high resolution and depth of imaging. LIF is not depth resolved, but a focused (small diameter) excitation beam enables a limited tissue volume to be interrogated.

2. Materials and methods

2.1 Proximal optics

A block diagram of the dual-modality system is shown in Fig. 1. While the optical paths of each modality were separated proximally, they were combined distally in the sample arm. The problem at hand was to not only combine the two unique systems in one endoscope, but also focus the two wavelengths achromatically.

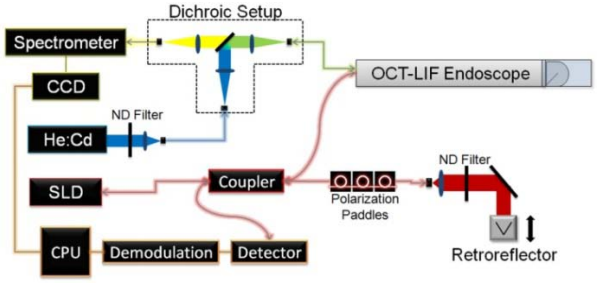

Fig. 1. Block diagram of the dual modality OCT-LIF subsystem, pictured with optional dichroic proximal optics setup (outlined). OCT (1300 nm center wavelength superluminescent diode (SLD)) and LIF (helium:cadmium (He:Cd) with 325 nm excitation wavelength) sources are fiber coupled into focused OCT-LIF endoscope. Neutral density (ND) filters attenuate source power, while spectrometer data is collected by a charge-coupled device (CCD) and electronically transmitted to the central processing unit (CPU).

2.1.1 OCT

The OCT subsystem was a conventional time-domain OCT system similar to one previously described in detail [28]. A superluminescent diode (SLD) source with a center wavelength of 1300 nm and a bandwidth of 64 nm (Superlum, Moscow, Russia) was coupled into the source arm of a fiber Michelson interferometer. The coherence length of the source was approximately 11.6 μm in air and 8.3 μm in tissue, assuming an average index of refraction, n = 1.4. The reference arm of the interferometer consisted of a galvanometer-mounted retroreflector providing 2 mm of pathlength modulation at 14 ascans/s. This slow speed was acceptable since the speed of the system was limited by the integration time necessary to acquire a strong autofluorescence signal. The sample arm of the interferometer is described subsequently. Interference then occurred when the path lengths of light reflected from the sample and the reference mirror were matched to within the coherence length of the source.

2.1.2 LIF

Our endoscope incorporated two LIF fibers, and could be configured to utilize single fiber for both excitation and emission, or to utilize separate excitation/emission fibers. It has been shown that the two geometries will result in different light collection efficiencies and tissue sampling depths [29]. As the separation between the excitation and emission fibers increases by a distance d, the penetration depth increases by a distance approximately d/2 [30]. As the separation increases however, the collection efficiency also decreases exponentially [31]. Therefore, the single channel design provided the least depth of penetration while also the greatest collection efficiency. We desired a penetration depth limited to the mucosa (~200 μm) and high collection efficiency, thus favoring the single-fiber configuration. However, due to the increased complexity of single fiber proximal optics, we tested both configurations. The LIF excitation source was a He:Cd laser, operating at 325 nm (Kimmon Electric, Centennial,

#134844 - $15.00 USD Received 14 Sep 2010; revised 4 Nov 2010; accepted 28 Jan 2011; published 31 Jan 2011

CO). A metalized neutral-density filter reduced the laser power before the light was directed through a 150 mm focal length fused-silica singlet to couple the laser light into an aluminum-jacketed multimode fiber, with a 200 μm core and a NA of 0.22. The power on the sample was approximately 1.2 mW.

2.1.2.1 Dual-fiber configuration

In the dual-fiber configuration, one endoscope LIF multimode fiber guided light from the laser to the distal optics and on to the tissue. Light emitted from the sample was collected with a second similar fiber. Fluorescent light from the proximal end of the emission fiber was then collimated with a 35 mm focal-length fused-silica singlet and directed through a dielectric-coated long pass filter to remove the excitation light. Resulting light was then focused onto the spectrometer (Spectrum-1 R08, HORIBA Jobin Yvon, Edison, NJ) using a 75 mm focal length BK7 singlet matched to the fiber NA.

2.1.2.2 Single-fiber configuration

Alternatively, a single fiber could be used for the excitation and emission, using a dichroic beamsplitter-based proximal optics design. Instead of coupling directly into the endoscope, laser light was coupled into a patch fiber which was fed into a dichroic proximal optics setup outlined in Fig. 1. Light from the patch fiber was collimated with a fused silica 75 mm focal length lens and incident upon a long-wave pass dichroic beamsplitter at 350 nm with high reflectivity at the laser wavelength, and a high transmission at slightly longer wavelengths (35-6923, Coherent, Santa Clara, CA). Specifically, for 325 nm excitation the characteristics were 95% reflection at 325 nm and transmission of 5% at 340 nm, 80% at 360, and greater than 90% at 375 to 700 nm. Reflected laser light was focused with another fused silica 75 mm focal length lens and coupled into a multimode fiber leading into the endoscope. This light was guided to the distal optics and focused onto the tissue. Emitted light from the tissue was collected with the same fiber, and propagated through the fiber in the opposite direction. The Stokes-shifted emitted light was transmitted by the beamsplitter. It was focused with a final fused silica 75 mm focal length lens and coupled into another multi-mode fiber which guided it to the spectrometer.

2.2 Distal sample arm optics

To achieve achromatic focusing of two different wavelengths of light, there were multiple potential options. Refractive optics have been used in high resolution, moderately large bandwidth endoscopes to focus light [8]. Simple refractive optics can encompass strong chromatic aberrations which would disallow their use for this purpose [32]. Multiple refractive components can mitigate chromatic aberration, however space, cost, and construction difficulty become concerns. A potentially simpler option was to use reflective focusing optics. Reflective optics are commonplace in telescopes and microscopes alike to focus light and achieve high resolution, but have yet to be widely utilized in endoscopes.

Chromatic aberration is absent in reflective optics designs [33]. When reflecting a large range of wavelengths, the reflecting material had to be taken into account. While silver and gold have excellent reflectivity above 1 μm, their low efficiency in the UV precluded use for this application. Aluminum was the most viable coating option because of its high efficiency across the UV-NIR wavelength range [34]. Highest efficiency could be achieved with total internal reflection (TIR). If uncoated reflections at glass-air interfaces could be utilized, the efficiencies of all wavelengths will be maximized with no light lost at the interface [35]. As with refractive optics, a symmetrical design using reflective optics would cause odd aberration terms to cancel out, most important coma [32].

The initial design constraint for the new endoscope was diameter. The packaging tube, distal optics, and outer envelope all had to be sufficiently small to fit inside the mouse colon, limiting the outer diameter of the system to smaller than about 2.1 mm. The thickness of the

#134844 - $15.00 USD Received 14 Sep 2010; revised 4 Nov 2010; accepted 28 Jan 2011; published 31 Jan 2011

envelope limited the diameter of the distal optics to about 1.8 mm. The radius of curvature of the ball lens was selected to be 1 mm, which enabled the lens to physically fit within this space while allowing for enough working distance to focus the light outside the endoscope envelope. Zemax (Zemax Development, Bellevue, WA) and ASAP (Breault Research, Tucson, AZ) optical modeling software were used to characterize beam propagation of the OCT and LIF optical paths through the distal optics. The optics for the sample arm were designed to not only achromatically focus both beams but also nearly coalign the OCT and LIF excitations beams, allowing for similar tissue regions to be inspected. The performance of the OCT channel was optimized in these designs, since wavefront quality and small beam waist are necessary for imaging. These optical models were formulated to calculate TIR tolerances of the lens, as well determine as the location and angle of the final folding mirror. Since TIR was not reliable at this surface, an aluminum coating was applied to maximize the system efficiency. The plane was oriented at a 40° angle (rather than 45°) to minimize back reflections from the lens and envelope. The placement of the OCT and LIF fibers was then optimized in order to obtain an acceptable focal location in the tissue while assuring TIR at the spherical lens surfaces. The cylindrical portion of the lens was set so that the fibers could be glued directly to the lens.

A reflective ball lens made of BK7 glass, as modeled in Fig. 2, with a diameter of about 1.8 mm was constructed to utilize TIR at two spherical surfaces and reflection at a third internal flat mirrored face to focus the beams onto the tissue. The initial single-element ball lens was not only ground down to modeled specifications, but was also cut in two as to allow for the aluminization of the third face to ensure reflection. Light diverging from the fibers (OCT NA = 0.14, LIF NA = 0.22) reflected off the first curved surface, which had a radius of curvature equal to 1 mm, and a focal length of about 0.33 mm. The light from the fiber was imaged to an intermediate focus inside the glass, diverged, and reflected off the second curved surface, which had identical properties to the first surface. The light reflected off of the 40 degree internal mirrored face, being directed downwards onto the tissue, and came to a focus 200 μm outside the ball lens and 30 μm outside a protective quartz envelope over the distal optics. The ball lens was a symmetrical 1:1 imaging system that obtains a theoretical diffraction-limited resolution for both the OCT (800-1300 nm) and LIF (325 nm or longer) channels.

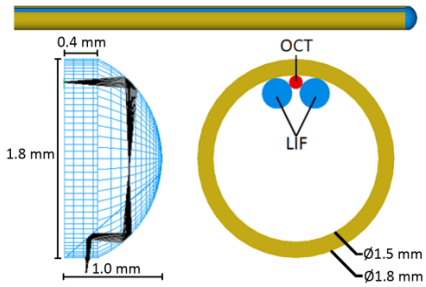

Fig. 2. Optical and mechanical design of Focused OCT-LIF Endoscope. Light from fibers secured along inside top surface of endoscope steel tube is focused and reflected downwards onto tissue with novel reflective ball lens design.

Using either LIF configuration, OCT and LIF excitation foci were separated by 100 μm circumferentially and 50 μm axially (Fig. 3). When the LIF fiber was placed adjacent to the OCT fiber (and thus off the axis of symmetry of the lens) aberrations affected the LIF spot shape. However, about 90% of the power was modeled to still be within the diffraction limit. The size of the LIF spot was also relatively large as limited by the multimode fiber core diameter.

#134844 - $15.00 USD Received 14 Sep 2010; revised 4 Nov 2010; accepted 28 Jan 2011; published 31 Jan 2011

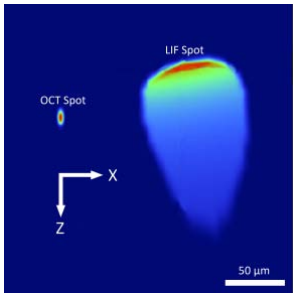

Fig. 3. OCT and LIF excitation spots at window. Spots are only separated by 100 µm circumferentially (x-axis) x 50 µm axially (z-axis).

2.3 Mechanical setup

2.3.1 Endoscope

A total of three fibers were secured near the top interface of the ball lens. The OCT fiber was first cemented to the uppermost inner side of a 1.5 mm inner-diameter, 1.8 mm outer-diameter steel tube. In order for the practical resolution and working distance of the OCT channel to match the modeled values, the OCT fiber was placed flush with the end of the tube and oriented exactly along the tube's longitudinal axis. Two LIF fibers were then fixed to flank the OCT fiber on either side. The ball lens was then attached directly to the tube with low-fluorescence UV curing epoxy, which also served as an index matching medium between the OCT fiber and lens. While it was nearly impossible to keep the epoxy from seeping into the LIF-lens interface, the epoxy showed negligible attenuation and autofluorescence at 325 nm for the micron scale thickness expected. A 40 mm long quartz envelope (1.9 mm ID, 2.1 mm OD) attached to a larger steel tube slid over the inner tube and ball lens assembly to provide protection and assure an air interface for proper TIR at the ball lens.

2.3.2 Translation stage

A longitudinal scan was achieved by translating the inner tube and endoscope distal optics through the length of the outer quartz envelope. The length of the longitudinal scan was limited by the quartz envelope to approximately 30 mm. Mechanical and software limits were applied to limit scan lengths and prevent possible damage to the distal optics from over-translation.

2.4 Data acquisition

LabVIEW software was used to synchronize reference arm movement with longitudinal translation, and simultaneous OCT data and LIF spectra acquisition, while also processing and displaying images. The spectrometer had an exposure time anywhere between 500 ms and 2 s, with an interval delay of ~500 ms for data transfer and computation time. The spectrometer CCD image was binned to yield a single spectrum for a single exposure. The endoscope catheter was calibrated and a system spectral response was developed using a calibrated light source (Ocean Optics, Dunedin, FL). The measured spectra were averaged in wavelength to match the spectral resolution of the spectrometer, and dark noise subtracted. Previously measured autofluorescence and background signal were subtracted from the filtered spectra, and the spectral response divided through.

2.5 Animal imaging

Control A/J and colon cancer model A/J AOM treated mice were imaged by the combined OCT-LIF endoscope. All mice were purchased from Jackson Laboratories (Bar Harbor, ME) and housed by University Animal Care in microisolators on a 12:12-h light-dark cycle with free access to water and standard laboratory chow. Protocols were approved by the University

#134844 - $15.00 USD Received 14 Sep 2010; revised 4 Nov 2010; accepted 28 Jan 2011; published 31 Jan 2011

of Arizona Insitutional Animal Care and Use Committee. AOM treated mice were treated with 10 mg/kg of azoxymethane purchased from Sigma-Aldrich Chemicals (St. Louis, MO, USA) subcutaneously once a week for 5 weeks, starting at 7 weeks of age. Mice were imaged 15 weeks post-treatment to allow disease development.

Mice were anesthetized with 2.5% Avertin, administered intraperitoneally. The endoscope was coated with lubricant and inserted into the anus with the mouse in a dorsal supine position. Room lights were turned off during measurements, though some ambient light from electronics and displays remained. A survey of the colon was obtained by taking eight 30-mm lateral scans with 45 degrees rotation between images. OCT images were obtained with 100 a-scans/mm, and LIF spectra with approximately 5 spectra/mm.

3. Results

3.1 Distal optics/resolution

The edge response method was used to calculate the actual lateral resolution and render a lateral modulation transfer function (MTF) of the constructed system [36]. The full-width half-max (FWHM) lateral resolution OCT resolution of the system was calculated to be about 6 μm. This experimental resolution matched the theoretical value of a 5.5 μm diffraction limited spot with a 1300 nm center wavelength source. Depth of focus for the system was calculated to be +/– 90 μm with the best focus located 30 μm outside the outer glass envelope. Analysis of the OCT MTF curve showed that the system could resolve about 80 lp/mm at 0.3 contrast. In similar fashion, the LIF FWHM lateral resolution was measured to be about 152 μm compared to theoretical 129.5 μm FWHM with a 200 μm core diameter fiber.

OCT axial resolution was measured to be 16 μm FWHM in air (11 μm in tissue), which compared favorably with the theoretical resolution of 11 μm. Sensitivity of 90.7 dB was measured at an imaging sample arm power of 1.925 mW. Dynamic range of the system was measured to be 66.0 dB, while an average dynamic range of 38 dB was measured in tissue samples.

The distal optics LIF throughput was measured to be about 34%, compared to the designed 70% efficiency. In double pass, this led to a laser-to-detector efficiency of only about 10%, not including quantum yield and fluorescence collection efficiency. Overall efficiency was further lowered due to losses at coupling interfaces.

Due to this low efficiency, the single fiber configuration was preferred. It was the configuration used during *in vivo* mouse trials.

3.2 In vivo imaging

In vivo data taken of an AOM-treated mouse showed differences between histologically normal colon tissue and adenoma in both modalities. In Fig. 4, normal colon and adenoma are shown in the same 30 mm long OCT image. In the normal regions of the tissue the boundary between the mucosa and submucosa could be clearly seen and was within our viewing depth, whereas disorganized structure and strong signal attenuation were seen in a region of large adenoma.

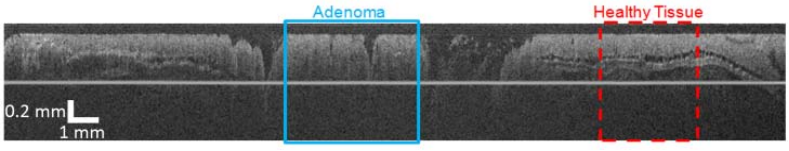

Fig. 4. OCT image of 30 mm long mouse colon acquired with new focused OCT-LIF Endoscope.

Averaged LIF autofluorescence emission spectra from normal and adenomatous regions of the colon are shown in Fig. 5. The normal spectrum had a peak intensity at about 440 nm,

#134844 - $15.00 USD Received 14 Sep 2010; revised 4 Nov 2010; accepted 28 Jan 2011; published 31 Jan 2011

whereas the spectrum for the adenoma was red-shifted with peak intensity at about 490 nm and peak intensity was attenuated by approximately 65%.

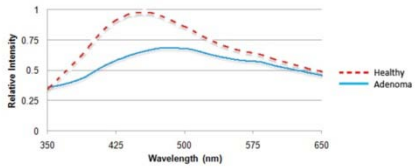

Fig. 5. LIF Spectra taken for healthy tissue and adenoma. For adenoma, the emitted fluorescence has a lower intensity and red shifted peak wavelength.

4. Discussion

A dual modality endoscope was built capable of achromatically focusing light over 325-1300 nm wavelength range. In practice, the endoscopic system was capable of achieving near-theoretical resolution during *in vivo* imaging. The healthy mouse colon is about 200-300 μm thick and thus the much of the healthy mouse colon (assuming apposition of the tissue with the endoscope) is within the depth of focus. Diseased colon and/or colon that is not in apposition results in required imaging depths outside the depth of focus. In practice, we notice some loss of lateral resolution and less signal at large depths, in comparison to existing OCT systems with a greater depth of focus. However, as illustrated in Fig. 4, we are able to identify all structures of the healthy mouse colon (mucosa, mucosa/submucosa boundary, and muscularis propria), as well as the lack of these structures in adenomatous tissue.

The line in the presented image is a result of the mutual coherence function (MCF) of the SLD source. The optical path distance from the OCT fiber-lens interface to the line in the image was measured to correspond to a secondary peak in the MCF. This line could be mitigated in future endoscopes by better index matching at the fiber-lens interface, creating an angled lens-fiber interface, or by choosing a different light source.

Astigmatism in the OCT channel introduced by the lack of symmetry of the sagittal and tangential light paths in the ball lens is reduced by use of the outer cylindrical window. We have previously examined the effects of a cylindrical probe envelope on astigmatism [27], and in general the use of thin envelopes—which act as negative lenses—and cylindrical inner optics reduces the astigmatism to manageable levels. In our case, optical models predicted an 8 μm x 3.3 μm spot size at best focus and axial waist separation of 19 μm. The envelope also acts to decrease the axial chromatic aberrations in the system, and the shift in foci between the 325 and 1300 nm spots is reduced to within the diffraction limit of the system. The choice of two different LIF configurations (single- or dual-fiber) enabled variable depth of imaging. The dual fiber setup demonstrated spatially separated emission and excitation areas, allowing us to inspect the biochemical distribution of deeper tissue. The dichroic proximal setup, on the other hand, displayed the shallowest penetration depth and had the greatest collection efficiency. Adenomas in the diseased mouse were detected by both modalities. Dual-modality imaging should raise the specificity and sensitivity of detection of precancerous tumors *in vivo* in mice. Both LIF fiber configurations can also be used for detecting biochemicals within the colon. Though fluorescence emission from collagen, NADH, and FAD, as well as oxyhemoglobin absorption are observed when tissue is excited with 325 nm light [11], the dichroic filter can be replaced in the single fiber setup to enable use of other excitation wavelengths, leading to the preferential excitement of different endogenous or exogenous fluorophores [37].

We are working on modifications and improvements to the endoscope in efforts to increase LIF channel throughput and reduce the beam size. With larger NA fibers being used for LIF as opposed to OCT, there were tighter practical assembly tolerances to ensure high efficiency TIR of LIF light. There are also some differences in optical performance between OCT and LIF channels that result from the size and placements of their respective fibers. The

#134844 - $15.00 USD Received 14 Sep 2010; revised 4 Nov 2010; accepted 28 Jan 2011; published 31 Jan 2011

center of the multimode fiber (LIF channels) is 78 μm closer to the central axis of the endoscope. Also, the angular displacement of the multimode fibers causes the LIF light to be obliquely incident on the fold mirror face. These differences lead to the LIF spot being highly aberrated. However, models predict that an estimated 95% of the energy is concentrated within measured FWHM of 152 μm, which is a greater than 5-fold increase in LIF resolution over our previous, unfocused, designs.

While the OCT light followed its prescribed course, inspection of our built endoscope showed a decreased throughput when compared to modeled efficiencies. In practice, roughly 65% of the light coupled into the LIF excitation fiber was not transmitted to the tissue surface. Ideally, all of the light from the LIF fibers reflects at the first interface in the ball lens, with all light being incident at an angle slightly greater than the TIR critical angle. Ultratight construction tolerances arise from the proximity of the incident ray angles to the critical angle, as there is less than a 3 degree acceptable deviation for TIR to occur. As a result, an unwanted 20% of LIF light was transmitted at the first TIR surface in practice.

Light that was transmitted at this interface also did not necessarily continue to follow the prescribed light path as another 5-10% of light was lost at the second TIR interface. Furthermore, an estimated 15% of LIF light was not reflected downwards by the internal mirror, and lost inside the body of the endoscope. Addition losses were attributed to unwanted reflections at the cut plane resulting from the construction of the lens, the absorption of light by unwanted epoxy at the fiber/lens interface, and specular reflections at the inner and outer surface of the endoscope window.

The most substantial losses were contributed to the failure of LIF light to TIR. While this is still theoretically the most efficient process for the ball lens, the practicality of such tight positioning tolerances make an aluminum coating on the lens more attractive. To quantify our assertions, we have coated the spherical surface of an endoscope ball lens with aluminum. We observed increased throughput of approximately 50% compared to 34%. However in coating the ball lens, stray light was trapped inside the distal end of the endoscope, and upon multiple reflections caused 7x higher autofluorescence of the endoscope coming from the increased fluorescence emission of the epoxy. Therefore, overall ability of the endoscope to detect a weak fluorescence signal was better with the uncoated endoscope. In future designs, the use of a slightly lower NA LIF fiber could relax positioning tolerances and lead to a practically more effective endoscope.

LIF spot size, and thus resolution, could be increased somewhat by choosing a smaller core diameter multimode fiber. For emission collection, however, large core diameter fibers are best, as collection efficiency is proportional to the square of the core diameter. Therefore, there are practical limits on the resolution of the LIF subsystem, at least when measuring weak autofluorescence signals.

The tomograms and spectra presented here clearly reveal adenoma formation in the living mouse without application of exogenous dyes. We expect the focused LIF channel to allow us to sense small focal regions of neoplasia better than our other existing endoscopes, however further studies are necessary to evaluate this hypothesis.

Acknowledgments

This research was supported in part by National Institutes of Health (NIH) grant ROICA109385.

#134844 - $15.00 USD Received 14 Sep 2010; revised 4 Nov 2010; accepted 28 Jan 2011; published 31 Jan 2011